Electrostatic instabilities driven by ion beams

Article *in* Plasma Physics and Controlled Fusion · September 1990

DOI: 10.1088/0741-3335/32/9/005

2 authors, including:

Pedro Vega
University of La Serena
13 PUBLICATIONS **55** CITATIONS

SEE PROFILE

Electrostatic instabilities driven by ion beams

1990 Plasma Phys. Control. Fusion 32 737

(http://iopscience.iop.org/0741-3335/32/9/005)

Plasma Physics and Controlled Fusion, Vol. 32, No. 9, pp. 737 to 757, 1990
Printed in Great Britain.

0741-3335/90 $3.00+ .00

ELECTROSTATIC INSTABILITIES DRIVEN BY ION BEAMS

L. GOMBEROFF and P. VEGA*
Departamento de Física, Facultad de Ciencias, Universidad de Chile, Casilla 653, Santiago, Chile

(*Received* 22 *August* 1989; *and in revised form* 9 *April* 1990)

Abstract—We consider electrostatic instabilities in a plasma composed of an ion beam moving in a stationary background of electrons and ions. Analytical expressions for the ion-acoustic and ion–ion acoustic instabilities are derived. These expressions consist of a system of two algebraic coupled equations, which do not shed much light on the nature of the unstable modes. However, when the system is complemented with the condition for marginal instability, they provide a simple graphic method to understand the nature of the instabilities. It is shown that kinetic Landau effects are responsible for the fact that the growth rate of the ion–ion acoustic instability can grow larger than the growth rate of the ion-acoustic mode. This result, which follows from the graphic method developed here, helps to resolve unambiguously an ongoing controversy concerning the nature of the ion–ion acoustic instability.

1. INTRODUCTION

DURING THE LAST few years, electrostatic instabilities generated by ion beams have received renewed attention. The reason for this is that beam velocity distributions and electrostatic instabilities associated with ion beams have been observed in various space plasmas (e.g. GARY and OMIDI, 1987 and references therein).

Following the observations of broadband electrostatic noise in the Earth's magnetotail (SCARF *et al.*, 1974; GURNETT and FRANK, 1977), GRABBE and EASTMAN (1984) proposed a mechanism based on the ion beam plasma instability in order to explain this noise. They could account for waves propagating parallel or almost parallel to the Earth's magnetic field, but the observations showed that the stronger emissions were produced nearly perpendicular to the magnetic field (GURNETT and FRANK, 1978). It was then shown (OMIDI, 1985; AKIMOTO and OMIDI, 1986) that large angle emissions are the result of the interaction between the ion beam and the ion core, while low angle emissions are due to the interaction between the ion beam and the electrons. The former instability, which has been called the ion–ion acoustic instability (GARY and OMIDI, 1987; AKIMOTO and OMIDI, 1986), has been studied by a number of authors (OMIDI, 1985; AKIMOTO and OMIDI, 1986; GARY and OMIDI, 1987; DUSENBERY and LYONS, 1985) using numerical solutions of the exact dispersion relations.

In spite of the fact that some earlier studies, based on analytical results (STRINGER, 1964; FRIED and WONG, 1966; FORSLUND and SHONK, 1970; GRESILLON *et al.*, 1975), have contributed to a deeper understanding of the ion–ion acoustic instability, there are still some questions concerning its nature.

Thus, while some people claim that it is a nonresonant fluid-like instability (OMIDI, 1985; AKIMOTO and OMIDI, 1986; OMIDI and AKIMOTO, 1988; GARY and OMIDI,

* Fellow of the Andes Foundation.

1987), others claim that it is a resonant kinetic-like instability (DUSENBERY and LYONS, 1985; DUSENBERG, 1986, 1987, 1988).

The origin of the discrepancy lies in the fact that most of the work done on the ion–ion acoustic instability is based on numerical solutions of the exact dispersion relation. From these studies, it is difficult to know the role played by the Landau factors in the dispersion relation. One way to settle this question is to derive an analytical expression for the dispersion relation so that the role played by the exponential terms of the plasma dispersion function (FRIED and CONTE, 1961) can be clearly discerned.

To this end, in Section 2 we derive analytical expressions for the dispersive properties and growth rates of the ion–ion acoustic and ion-acoustic instabilities. The resulting equations are not very transparent in the sense that they describe, simultaneously, the two modes. In order to separate the main effects leading to each mode, in Section 3 we derive a method which involves the marginal instability condition. It is also shown that the equations are in very good agreement with exact numerical results. The method allows for an easy understanding of the properties of each mode and of the role played by the Landau factors. In Section 4, we show that the equations derived in Section 2 reduce to the well-known dispersion relation for ion-acoustic waves propagating parallel, or almost parallel to the ion beam. In Section 5 we summarize the main results.

2. THEORY

We shall consider a plasma composed of a stationary population of electrons and ions described by Maxwellian distribution functions, and an ion beam described by a drifting Maxwellian with drift velocity **U**.

Under these conditions, the dispersion relation for electrostatic waves in a homogeneous, unmagnetized plasma is given by (OMIDI, 1985):

$$1 = \frac{\omega_{pe}^2}{k^2\alpha_e^2} Z'\left(\frac{\omega}{k\alpha_e}\right) + \frac{\omega_{pi}^2}{k^2\alpha_i^2} Z'\left(\frac{\omega}{k\alpha_i}\right) + \frac{\omega_{pb}^2}{k^2\alpha_b} Z'\left(\frac{\omega - k_\parallel U}{k\alpha_b}\right), \tag{1}$$

where Z is the dispersion function of FRIED and CONTE (1961), $k_\parallel$ is the projection of the wave vector **k** along the drift velocity **U**, and α_l the thermal velocity for $l = e, i, b$.

Assuming $\omega = \omega_r + i\gamma$ with $\omega_r \gg \gamma$, a Taylor series expansion of the plasma dispersion function to first order in γ yields:

$$Z\left(\frac{\omega}{k\alpha}\right) = Z\left(\frac{\omega_r}{k\alpha}\right) + \frac{i\gamma}{k\alpha} Z'\left(\frac{\omega_r}{k\alpha}\right). \tag{2}$$

Assuming $\omega/k\alpha_e \ll 1$, $\omega/k\alpha_i \gg 1$ and $|\omega - k_\parallel U|/k\alpha_b \gg 1$, and using the Taylor series expansion of the dispersion function for the electron background and the asymptotic expansion for the ion core and the ion beam, equation (1) yields the following equations for ω_r and γ:

$$y^2 = -2\left(\frac{U}{\alpha_e}\cos\theta\right)^2 + \frac{\delta\eta_b}{\left(1-\frac{x}{y}\right)^2}\left[1+\frac{3}{2}\frac{1}{\left(\frac{U}{\alpha_b}\cos\theta\right)^2\left(1-\frac{x}{y}\right)^2}\right]$$

$$+\frac{\delta\eta_i}{\left(\frac{x}{y}\right)^2}\left[1+\frac{3}{2}\frac{1}{\left(\frac{x}{y}\frac{U}{\alpha_i}\cos\theta\right)^2}\right]$$

$$+\frac{2\delta\eta_b\sqrt{\pi\gamma}}{y\omega_{pe}}\left(\frac{U}{\alpha_b}\cos\theta\right)^3\left[1-2\left(1-\frac{x}{y}\right)^2\left(\frac{U}{\alpha_b}\cos\theta\right)^2\right]e^{-\left(1-\frac{x}{y}\right)^2\left(\frac{U}{\alpha_b}\cos\theta\right)^2}$$

$$+\frac{2\delta\eta_i\sqrt{\pi\gamma}}{y\omega_{pe}}\left(\frac{U}{\alpha_i}\cos\theta\right)^3\left[1-2\left(\frac{x}{y}\frac{U}{\alpha_i}\cos\theta\right)^2\right]e^{-\left(\frac{x}{y}\frac{U}{\alpha_i}\cos\theta\right)^2}, \tag{3}$$

and

$$\frac{\gamma}{\omega_{pe}} = \sqrt{\pi}x\left(\frac{U}{\alpha_e}\cos\theta\right)^3\left\{e^{-\left(\frac{x}{y}\frac{U}{\alpha_e}\cos\theta\right)^2}+\delta\eta_i\left(\frac{\alpha_e}{\alpha_i}\right)^3\right.$$

$$\times e^{-\left(\frac{x}{y}\frac{U}{\alpha_i}\cos\theta\right)^2}-\delta\eta_b(\alpha_e/\alpha_b)^3\left(\frac{y}{x}-1\right)$$

$$\left.\times e^{-\left(1-\frac{x}{y}\right)^2\left(\frac{U}{\alpha_b}\cos\theta\right)^2}\right\}\Bigg/\left\{\frac{\delta\eta_b}{\left(1-\frac{x}{y}\right)^3}\left(1+\frac{3(\alpha_b/U)^2}{\left(1-\frac{x}{y}\right)^2\cos^2\theta}\right)\right.$$

$$\left.-\frac{\delta\eta_i}{(x/y)^3}\left(1+\frac{3(\alpha_i/U)^2}{(x/y)^2\cos^2\theta}\right)\right\}; \tag{4}$$

where

$$x = \frac{\omega_r}{\omega_{pe}}, \quad y = k_\parallel U/\omega_{pe}, \quad \cos\theta = k_\parallel/k,$$

$$\delta = m_e/m_i, \quad \eta_i = n_i/n_e, \quad \eta_b = n_b/n_e \quad \text{and} \quad \eta_i+\eta_b = 1.$$

The assumption that $\omega_r \gg \gamma$ will be justified *a posteriori*. The other assumptions depend mostly on the external parameters chosen, and although sometimes the ion background term approaches the strong resonance condition $\omega \simeq k\alpha_i$, it occurs close to the marginal frequency where not only is it unimportant but also, as we shall see, the approximations continue to be good. In the last part of the next section, the ion core temperature will be increased and $\omega/k\alpha_i$ will become less than 1. In such cases, equations (3) and (4) have to be changed accordingly.

Two electrostatic modes take place in the system. One is due to the relative drift between the two ion components, and shall be called the ion–ion acoustic instability after GARY and OMIDI (1987). The other mode is driven by the relative drift between the electron core and the ion beam and will be called the ion acoustic instability.

Equations (3) and (4) are approximate equations, valid under the afore-mentioned conditions and, as will be shown, are in very good agreement with exact numerical results.

Even though these equations are easy to handle, there is an exact relation that can be obtained from equation (1) by setting $\gamma = 0$, which corresponds to the condition for marginal instability. Thus, by setting $\gamma = 0$ in equation (1), we obtain from the imaginary part, the following condition for marginal instability:

$$e^{-\left(\frac{x}{y}\frac{U}{\alpha_e}\cos\theta\right)^2} + \delta\eta_i\left(\frac{\alpha_e}{\alpha_i}\right)^3 e^{-\left(\frac{x}{y}\frac{U}{\alpha_i}\cos\theta\right)^2} - \delta\eta_b\left(\frac{\alpha_e}{\alpha_b}\right)^3\left(\frac{y}{x}-1\right)e^{-\left(1-\frac{x}{y}\right)^2\left(\frac{U}{\alpha_b}\cos\theta\right)^2} = 0. \qquad (5)$$

The first term in this expression represents the electrons, the second term the ion background, and the third term the ion beam. The condition that the sum be equal to zero determines the marginal frequency. However, equation (5) not only determines the marginal frequency but, as we shall see, it also contains most of the relevant information concerning the ion acoustic and the ion–ion acoustic instability.

First, we notice that equation (5) depends on x and y only through the ratio x/y and that there are growing solutions for $x < y$ only. This means that the waves are unstable only when $U\cos\theta > v_{\text{phase}}$. Notice that $x/y = v_{\|\text{phase}}/U$.

3. MARGINAL INSTABILITY ANALYSIS

The three terms of equations (5) behave as shown in Fig. 1(a), where e, i and b refer to the electrons, background ions, and ion beam, respectively. The electronic term is of the order one for $(\omega/k\alpha_e) \ll 1$, throughout the interval $0 < (x/y) < 1$. The intersections between curve (e) and (b) and curve (i) and (b) give the marginal (x/y) values for the ion acoustic and ion–ion instability, respectively. The waves grow for (x/y) values less than the corresponding marginal values, that is, to the left of the intersections. Decreasing (x/y) values correspond to decreasing frequencies.

In Fig. 1(a), we have plotted the three terms of equation (5) for a plasma characterized by the parameters specified in the figure, which are the same as in Fig. 1 of GRABBE (1987) for two angles, $\theta = 0°$ and $\theta = 75°$. The first term, representing the electrons and denoted by (e), is insensitive to angle variations. The second term, representing the background ions, opens up as θ increases from 0° [curve (i)] to 75° [curve (i′)]. The third term, representing the beam, grows and widens with increasing θ. For $\theta = 0°$ this curve has been denoted by the letter (b) and for $\theta = 75°$ by (b′). For $\theta = 0°$, curves (e) and (b) intersect each other at $(x/y) \simeq 0.91$, where the two curves take the value 1. From the intersection point down to the value $(x/y) = 0.2$, curve (i) remains negligibly small compared to curve (e). Since the intersection gives the marginal mode and the waves grow to the left of the intersection, we conclude that the dominant instability is the ion acoustic instability. Actually, the marginal mode is given by the intersection of curves (e) + (i) with curve (b), but as explained above, curve (i) can be neglected with respect to curve (e) until $(x/y) \simeq 0.2$, where, as we shall see, the waves are damped.

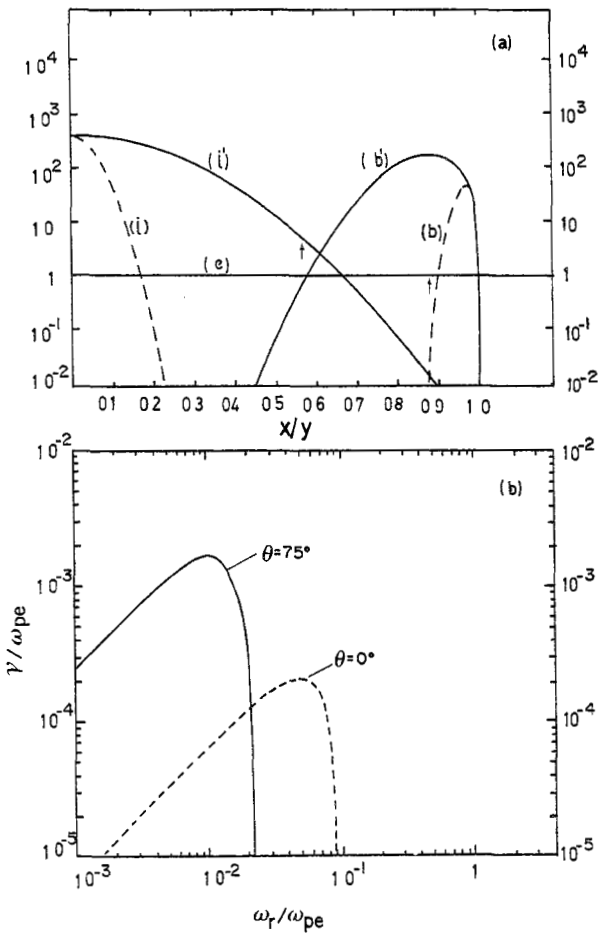

FIG. 1.—(a) The behavior of each term in equation (15) as a function of $(x/y) = V_{\parallel \text{phase}}/U$. Curve (e) corresponds to the electrons, and curves (i) and (b) to the ion core and ion beam, respectively. (b) Growth rates versus frequency normalized to ω_{pe}. The plasma parameters are $\eta_i = \eta_b = 0.5$, $(U/\alpha_i) = 14.3$, $(U/\alpha_b = 25$ and $(U/\alpha_e) = 0.12$ for $\theta = 0°$ (— —) and $\theta = 75°$ (——).

For $\theta = 75°$ the situation is completely different. Curves (i′) and (b′) intersect each other at $(x/y) \simeq 0.61$ at a value larger than 1, and curve (i′) continues to grow to the left of the intersection, showing that now the dominant instability is the ion–ion acoustic instability. Notice that curve (i′) at $(x/y) \simeq 0.5$ is already over one order of magnitude larger than the electronic term, curve (e).

In Fig. (1b) we have plotted the growth rates versus the frequency, both normalized to the electron plasma frequency for the two cases of Fig. 1(a). The growth rates have been calculated from equations (3) and (4) and we see that not only are they in good agreement with the exact numerical calculations of Fig. (1) of GRABBE (1987), but also they behave in the way anticipated in our Fig. 1(a). The arrows in

Fig. 1(a) correspond to the (x/y) value for $\gamma = \gamma_{max}$. We see that the range of (x/y) values from the marginal frequency to the frequency at which γ is maximum is very small, implying that as the growth rate increases from zero up to the maximum value, x/y remains almost constant. Actually, x/y is almost constant throughout the unstable frequency range, being constant of the order one for the ion acoustic mode, and of the order 1/2 for the ion–ion acoustic instability (see GRABBE, 1987; AKIMOTO and OMIDI, 1986).

3.1. *Sensitivity to beam temperature variations*

In Fig. 2(a), the beam temperature has been reduced, keeping the other parameters fixed as in figure 4 of GRABBE (1987). We have drawn again the three terms of equation (5) for $\theta = 0°$, 60° and 75°. As a consequence of the reduction in beam temperature, the term representing the beam grows and steepens, peaking closer to $(x/y) = 1$.

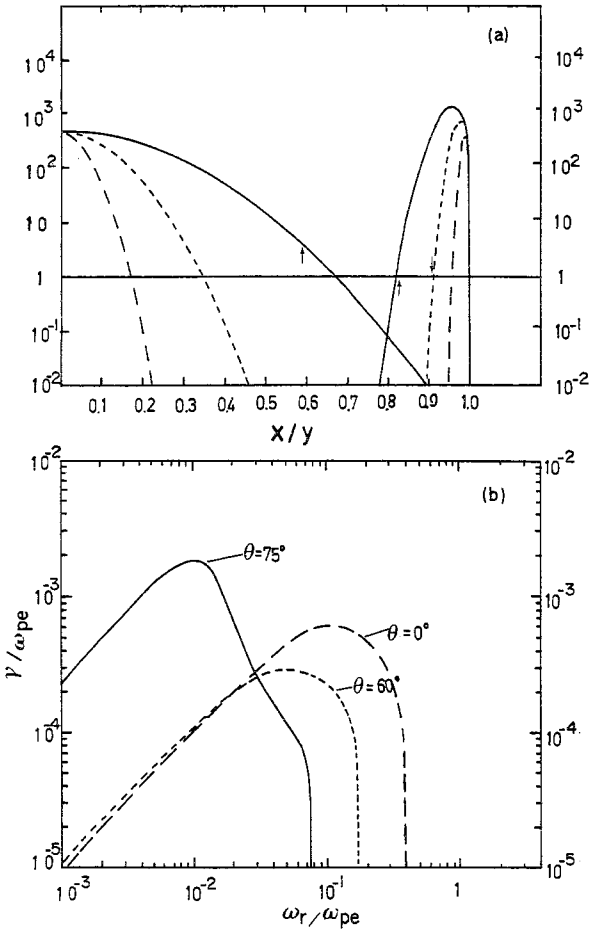

FIG. 2.—The same as Fig. 1 but for a colder beam with $(U/\alpha_b) = 66.67$ for $\theta = 0°$ (— —), 60° (- - - - -) and 75° (——).

As a result, the marginal mode occurs for higher (x/y) values, thus leading to an enhancement of the unstable spectra. Clearly the cases corresponding to $\theta = 0°$ and $60°$ are dominated by the ion acoustic instability. For $\theta = 75°$, the instability starts as an ion acoustic instability because at the marginal x/y value, the ion core term is over one order of magnitude less than the electronic term. However, at $(x/y) \simeq 0.67$ the electronic and ion background terms become equal and from there on the ion background term takes over, indicating a transition to the ion–ion acoustic instability. In Fig. 2(b) we have plotted the corresponding growth rates. We see that everything occurs as expected. Moreover, for $\theta = 75°$ the irregular increase of the growth rate to its maximum value can now be understood as being due to the transition from one instability to the other. If we compare our Fig. 2(b) with figure 4 of GRABBE (1987), we see that the agreement for $\theta = 0°$ is very good. However, for $\theta = 60°$ there is no agreement. In our case, the instability is ion acoustic whose maximum value occurs at $\theta = 0°$. In figure 4 of GRABBE (1987), the instability for $\theta = 60°$ is the ion–ion acoustic instability. However, according to the marginal condition, equation (5), a reduction in the beam temperature increases the angular threshold of the ion–ion acoustic instability, an effect which can be clearly inferred from our Figs 1(a) and 1(b). In fact, since the ion beam term shrinks with decreasing beam temperature, a larger angle is required in order that the ion core term intersects the beam term at a value close to, or larger than 1. Even for $\theta = 75°$, the instability begins as the ion acoustic, and only at $(x/y) \simeq 0.5$ starts turning into the ion–ion acoustic instability, as explained before. Our results are in agreement with OMIDI (1985), where it is shown that decreasing beam temperature increases the angle for which the maximum growth rate of the ion–ion acoustic instability takes the largest value.

As in Fig. 1(a), in Fig. 2(a) the arrows indicate the location of the corresponding maximum growth rates. The larger range of (x/y) values for the case of $\theta = 75°$ not only indicates a slower increase of the growth rate to its maximum value, but also a transition from the ion acoustic regime $x \simeq y$, to the ion–ion acoustic regime, $x \simeq \frac{1}{2}y$.

In Fig. 3(a), we have further decreased the beam temperature to $(U/\alpha_b) = 2 \times 10^3$, in order to show explicitly that larger angles are required to trigger the ion–ion acoustic instability. We have considered $\theta = 0°$, $75°$ and $85°$.

A comparison between Figs 2(a) and 3(a) shows that the term representing the beam continues to grow and shrink, implying a larger angular threshold for the ion–ion acoustic instability. In Fig 3(b), we show the corresponding growth rates. For $\theta = 75°$, the ion–ion acoustic instability overcomes the ion acoustic instability very close to the maximum growth rate, while for $\theta = 85°$ this is dominant throughout the unstable frequency range.

Hence, we conclude first that by decreasing the beam temperature, the marginal frequency for any angle increases leading thereby to broader spectra; secondly, the ion–ion acoustic instability dominates over the ion acoustic instability with increasing angles. However, even though the angle can get very close to 90°, it can never be equal to 90° because the growth rate is proportional to $\cos^3 \theta$ [see equation (4)]. We shall come back to this point later.

3.2. *Sensitivity to ion core temperature variations*

Let us now study the effect of varying the background ion temperature. To this end, in Fig. 4(a) we have increased the ion core temperature from $(U/\alpha_i) = 16.67$ to

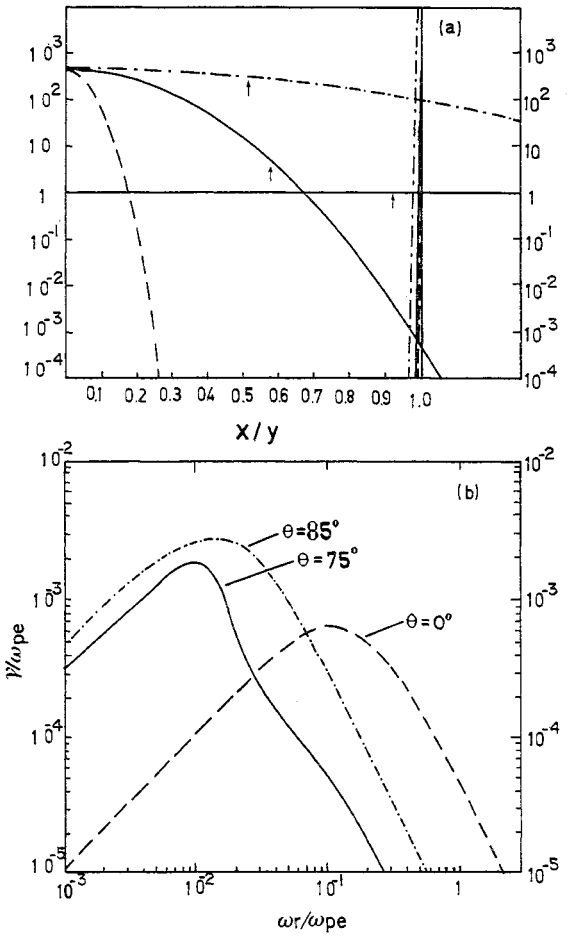

FIG. 3.—The same as Fig. 1 but for a very cold beam with $(U/\alpha_b) = 2 \times 10^3$ for $\theta = 0°$ (——), 75° (——) and 85° (-·-·-·).

$(U/\alpha_i) = 5.9$, for fixed $\theta = 75°$. The other parameters are as in Fig. 1. From equation (5) it follows that at $(x/y) = 0$, the term representing the background ions is given by $\delta\eta_i(\alpha_e/\alpha_i)^3$, so that the effect of increasing α_i is to reduce this term at $(x/y) = 0$. Although for $(U/\alpha_i) = 5.9$ the intersection between this term and the term representing the beam is larger than for the case when $(U/\alpha_i) = 16.67$, from Fig. 4(b) it follows that the maximum growth rate is almost one order of magnitude larger for the colder case. This is readily understood by noticing that the growth rate depends on the difference between the ion background term and the ion beam term, and we see that at the position of the maximum, shown by the arrows in Fig. 4(a), the difference for the colder case is larger. However, in both cases the dominant mode is the ion–ion acoustic instability.

It is important to notice that as a result of the ion core temperature increase, $(\omega/k\alpha_i)$ is now smaller than 1, and thus equations (3) and (4) are no longer valid because they

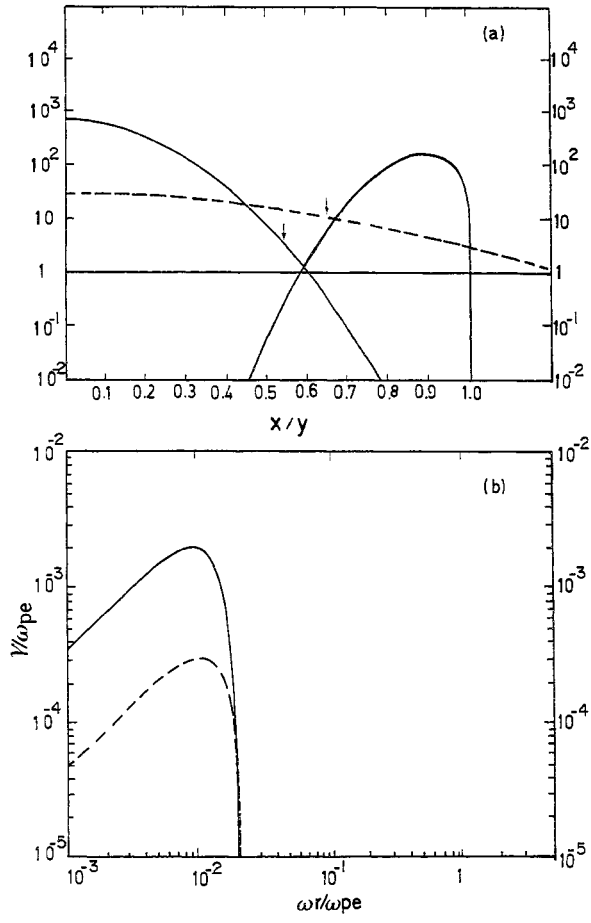

FIG. 4.—The same as Fig. 1 but for two ion core temperatures, $(U/\alpha_i) = 16.67$ (——) and $(U/\alpha_i) = 5.9$ (— —) for $\theta = 75°$.

have been obtained by using the large argument expansion of $Z(\omega/k\alpha_i)$. However, by using the expansion of $Z(\omega/k\alpha_i)$ for small values of the argument, we obtain

$$y^2 = -2\left(\frac{U}{\alpha_e}\cos\theta\right)^2 - 2\delta\eta_i\left(\frac{U}{\alpha_i}\cos\theta\right)^2\left[1-2\left(\frac{x}{y}\frac{U}{\theta_i}\cos\theta\right)^2\right]$$

$$+\frac{\delta\eta_b}{\left(1-\frac{x}{y}\right)^2}\left[1+\frac{3}{2}\frac{1}{\left(1-\frac{x}{y}\right)^2\left(\frac{U}{\alpha_b}\cos\theta\right)^2}\right]$$

$$+\frac{2\delta\eta_i\sqrt{\pi\gamma}}{y\omega_{pe}}\left(\frac{U}{\alpha_i}\cos\theta\right)^3\left[1-2\left(\frac{x}{y}\frac{U}{\alpha_i}\cos\theta\right)^2\right]e^{-\left(\frac{x}{y}\frac{U}{\alpha_i}\cos\theta\right)^2}$$

$$+\frac{2\delta\eta_b\sqrt{\pi\gamma}}{y\omega_{pe}}\left(\frac{U}{\alpha_b}\cos\theta\right)^3\left[1-2\left(1-\frac{x}{y}\right)^2\left(\frac{U}{\alpha_b}\cos\theta\right)^2\right]e^{-\left(1-\frac{x}{y}\right)^2\left(\frac{U}{\alpha_b}\cos\theta\right)^2}, \tag{6}$$

and

$$\frac{\gamma}{\omega_{pe}}=\sqrt{\pi x}(U/\alpha_e)^3\cos^3\theta\left\{e^{-\left(\frac{x}{y}\frac{U}{\alpha_e}\cos\theta\right)^2}+\delta\eta_i\left(\frac{\alpha_e}{\alpha_b}\right)^3 e^{-\left(\frac{x}{y}\frac{U}{\alpha_i}\cos\theta\right)^2}\right.$$

$$\left.-\delta\eta_b\left(\frac{\alpha_e}{\alpha_b}\right)^3 e^{-\left(1-\frac{x}{y}\right)^2\left(\frac{U}{\alpha_i}\cos\theta\right)^2}\right\}\Bigg/\left\{4\delta\eta_i\frac{x}{y}\left(\frac{U}{\alpha_i}\cos\theta\right)^4\left[1-\frac{4}{3}\left(\frac{x}{y}\frac{U}{\alpha_i}\cos\theta\right)^2\right]\right.$$

$$\left.+\frac{\delta\eta_b}{\left(1-\frac{x}{y}\right)^3}\left[1+\frac{3}{\left(\frac{U}{\alpha_b}\cos\theta\right)^2\left(1-\frac{x}{y}\right)^3}\right]\right\}. \tag{7}$$

The growth rate of Fig. 4(b) corresponding to $(U/\alpha_i) = 5.9$ was obtained by using equations (6) and (7).

In order to check the validity of equations (6) and (7), Fig. 5(a) shows the growth rate for the plasma model of Fig. 3 of OMIDI (1985) for $\theta = 0°$ and $75°$. A comparison between our Fig. 5(a) and his figure 3 shows good agreement between his exact numerical calculation and our results, based on equations (6) and (7). The agreement is not so good, however, for frequency values very close to the marginal frequency because at such frequencies, $(\omega/k\alpha_i)$ approaches the resonance condition $\omega \simeq k\alpha_i$. In Fig. 5(b) we show the behaviour of the terms of equation (5) for the plasma parameters of Fig. 5(a). It is clear that for $\theta = 75°$, the ion–ion acoustic instability is the dominant instability.

We have already seen that the angular threshold of the ion–ion acoustic instability increases for decreasing beam temperatures. Therefore, we expect the maximum growth rate, $\gamma_m(\theta)$, to be an increasing function of θ for decreasing beam temperatures. However, since $\gamma(\theta = 90°) = 0$, there must be an angle $\theta = \theta_{op}$ for which $\gamma_m(\theta_{op})$ is maximum. This angle can be approximately determined from the condition [see equation (4)]:

$$\frac{d}{d\theta}\left[\cos^3\theta\, e^{-\left(\frac{x}{y}\frac{U}{\alpha_i}\cos\theta\right)^2}\right]=0, \tag{8}$$

which yields

$$\cos\theta_{op}=\frac{3}{2}\left(\frac{y}{x}\right)_m\frac{\alpha_i}{U}. \tag{9}$$

Here $(y/x)_m$ is the value of y/x at which $\gamma = \gamma_m$. The value of θ_{op} clearly depends on U/α_i, but it also depends on U/α_b through the factor $(y/x)_m$, and this factor decreases with decreasing beam temperatures.

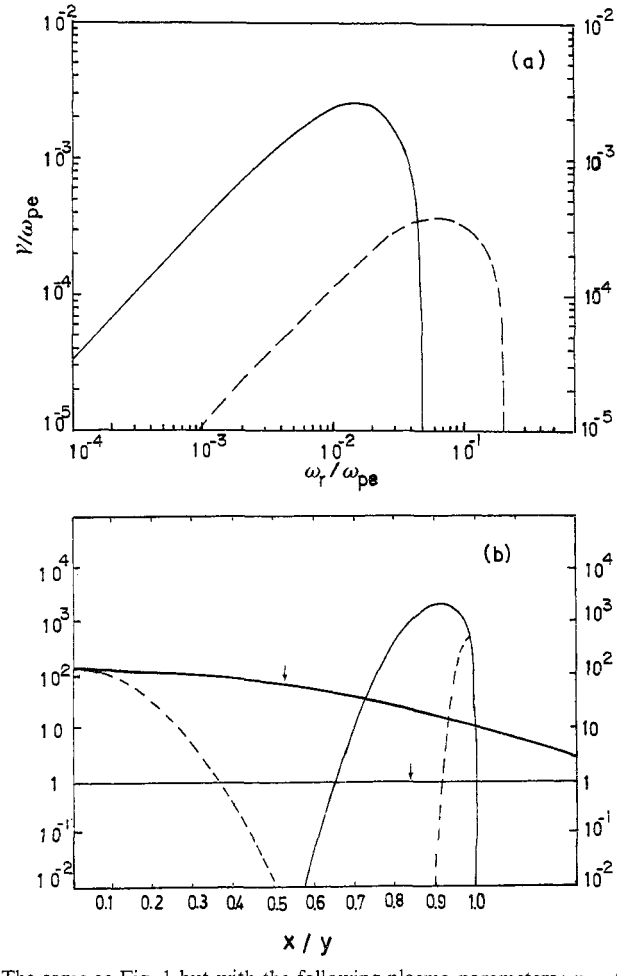

FIG. 5.—The same as Fig. 1 but with the following plasma parameters: $\eta_i = 0.4$, $\eta_b = 0.6$, $(U/\alpha_i) = 6.08$, $(U/\alpha_b) = 35.35$, and $(U/\alpha_e) = 0.07$ for $\theta = 0°$ (— —) and 75° (——).

In order to illustrate these results, in Fig. 6(a) we considered a plasma with $(U/\alpha_e) = 0.12$, $(U/\alpha_i) = 14.3$ and 20, and a very cold beam with $(U/\alpha_b) = 2 \times 10^2$. The angle was fixed at $\theta = 87°$. We see that the terms representing the ion background were flattened to almost the constant value $\delta\eta_i(\alpha_e/\alpha_i)^3$, i.e. the value they would reach at $\theta = 90°$. Clearly the dominant instability is the ion–ion acoustic instability. In Fig. 6(b) we show the corresponding growth rates and see that γ_{max} for $(U/\alpha_i) = 20$ is larger than for $(U/\alpha_i) = 14.3$. This result shows that θ_{op} has increased due to the reduction of the beam temperature, in agreement with equation (9).

In Fig. 7(a) we have fixed the ion core temperature and varied the beam temperature for $\theta = 85°$. From Fig. 7(b), we see that γ_{max} is larger for the colder beam as a result of the decrease in $(y/x)_m$, implying a larger θ_{op} which is in agreement with equation (9) and our previous considerations. Notice that $(x/y)_m = 0.47$ for the hotter beam and 0.52 for the colder beam.

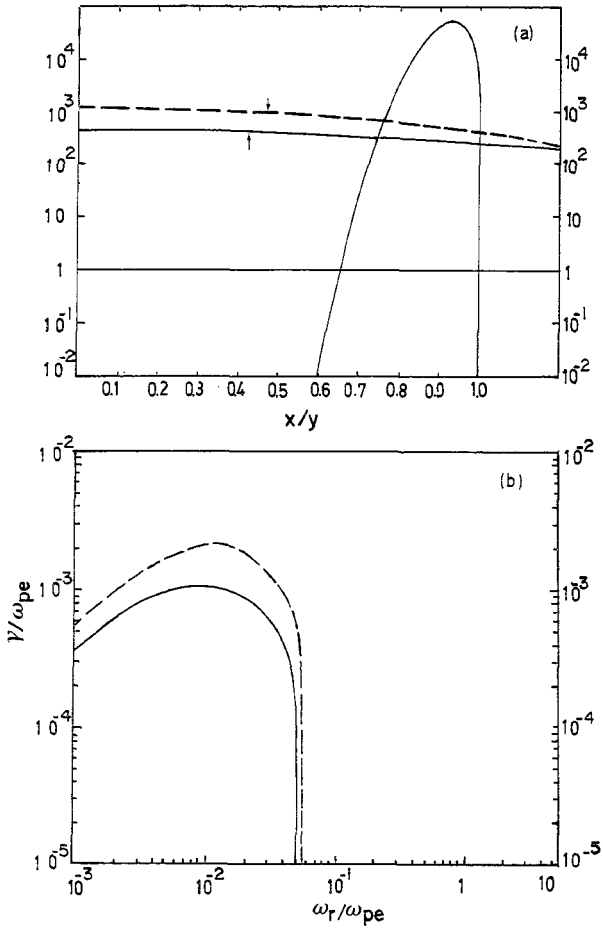

FIG. 6.—The same as Fig. 1 but for $\eta_i = \eta_b = 0.5$, $(U/\alpha_b) = 200$, $(U/\alpha_e) = 0.12$, $(U/\alpha_i) = 20$ (— —) and $(U/\alpha_i) = 14.3$ (——) for $\theta = 87°$.

3.3. *Sensitivity to ion density variations*

Let us now study the effect of varying the concentration of the ion background. To this end, in Fig. 8(a) we have taken the same plasma model as in Fig. 1, but η_i was varied from 0.5 to 0.01. From equation (5) it follows that η_i is a scale factor so that a change in η_i leads to a constant shift of the ion core term. A similar situation occurs for the beam term for which η_b is also a scale factor and, since η_i decreases when η_b increases, the ion beam term increases. From the figure, we see that as η_i decreases the instability, which for $\eta_i = 0.5$ is the ion–ion acoustic instability, for $\eta_i = 0.1$ intersects the corresponding beam term very close to 1. In other words, as η_i decreases, the instability is turning into the ion acoustic instability in such a way that for $\eta_i = 0.01$ it has completely turned into the ion acoustic instability. From the corresponding growth rates shown in Fig. 8(b), it is clearly seen that indeed for $\eta_i = 0.1$, the maximum growth rate of the ion–ion acoustic instability for $\theta = 75°$ becomes of the same order

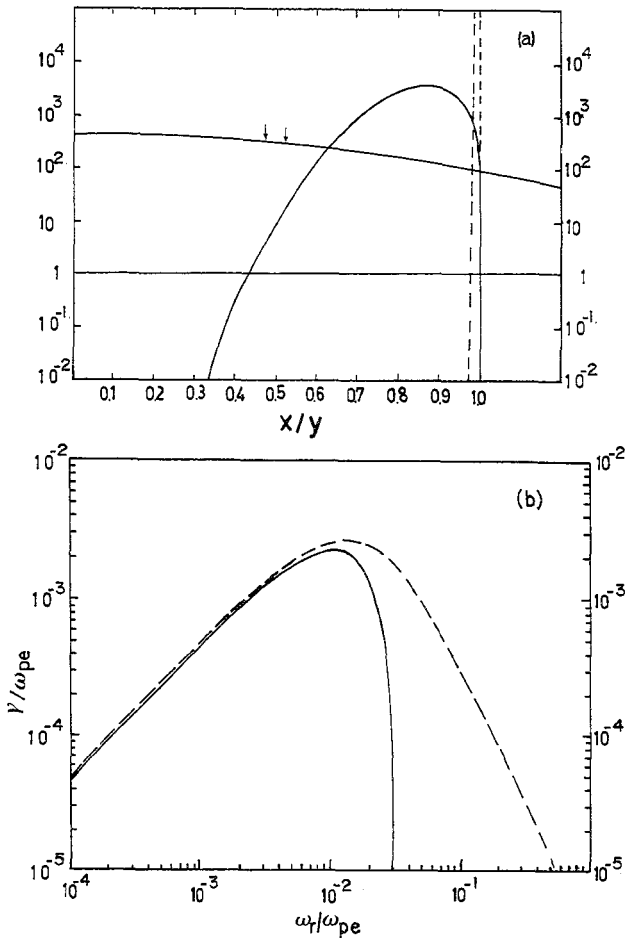

FIG. 7.—The same as Fig. 1 but for $(U/\alpha_b) = 66.67$ (——) and $(U/\alpha_b) = 2\times10^3$ (— —) for $\theta = 85°$.

of magnitude as the maximum growth rate of the ion acoustic instability for $\theta = 0°$; and for $\eta_i = 0.01$, it is the ion acoustic instability which is the dominant mode even for $\theta = 75°$. The maximum growth rate of this mode increases, reaching its largest value at $\theta = 0°$ [see Fig. 8(b)].

In Fig. 9(a) we have increased the concentration of the ion core from 0.5 to 0.9. One could think that increasing the ion core concentration beyond $\eta_i = 0.5$ might favour the ion–ion acoustic instability over the ion acoustic instability. However, from Fig. 9(b) it follows that when η_i is increased beyond 0.5, the maximum growth rate of the ion–ion acoustic instability decreases. This result is simple to understand by noticing that the ion–ion acoustic instability is due to the relative drift between the two ion populations and, since η_i increases as η_b decreases, from symmetry considerations it follows that the instability is maximum when $\eta_i = \eta_b$.

On the other hand, since the ion acoustic instability is due to the relative drift

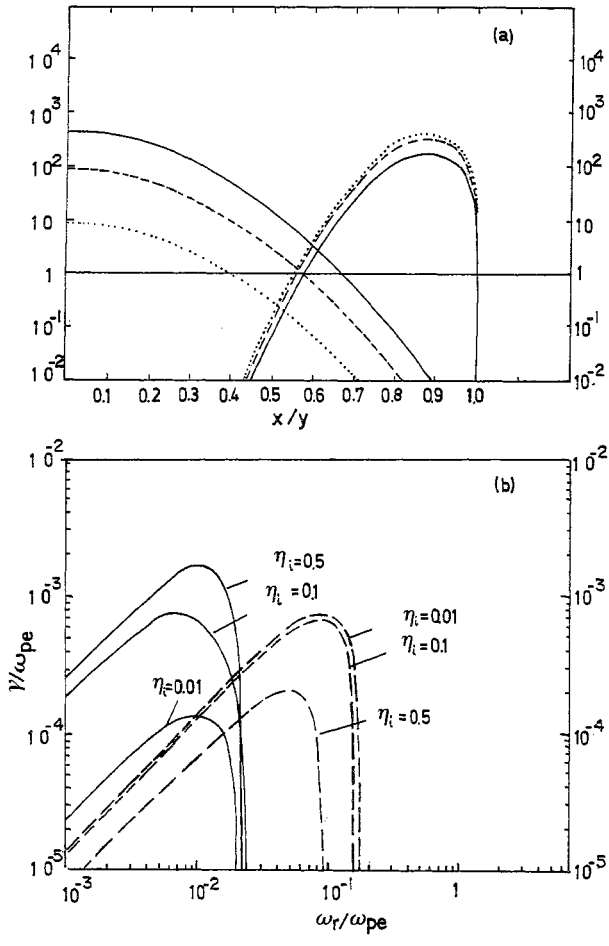

FIG. 8.—(a) The same as Fig. 1(a) but for varying ion core concentrations: $\eta_i = 0.5$ (——), 0.1 (— —) and 0.01 (.....). The angle is $\theta = 75°$. (b) Growth rates versus frequency normalized to ω_{pe} for $\theta = 0°$ (— —) and 75° (——). The other parameters are as in Fig. 8(a).

between the electrons and the ion beam, we expect the ion acoustic instability to be maximum in the absence of background ions; that is, for $\eta_i = 0$. These results are shown in Figs 8(b) and 9(b).

The result that the ion–ion instability is at a maximum for $\eta_i = 0.5$ can also be inferred from Figs 8(a) and 9(a). In fact, from the two figures it follows that the largest value of the intersection between the ion background term and the ion beam term occurs at $\eta_i = 0.5$, implying that the ion–ion acoustic instability is maximum for that value.

3.4. *Sensitivity to drift velocity variations*

Finally, in Fig. 10(a) we study the effect of varying the relative drift velocity. We have used the plasma model of Fig. 1, namely $U/\alpha_e = 0.12$, $U/\alpha_i = 14.3$ and $U/\alpha_b = 25$.

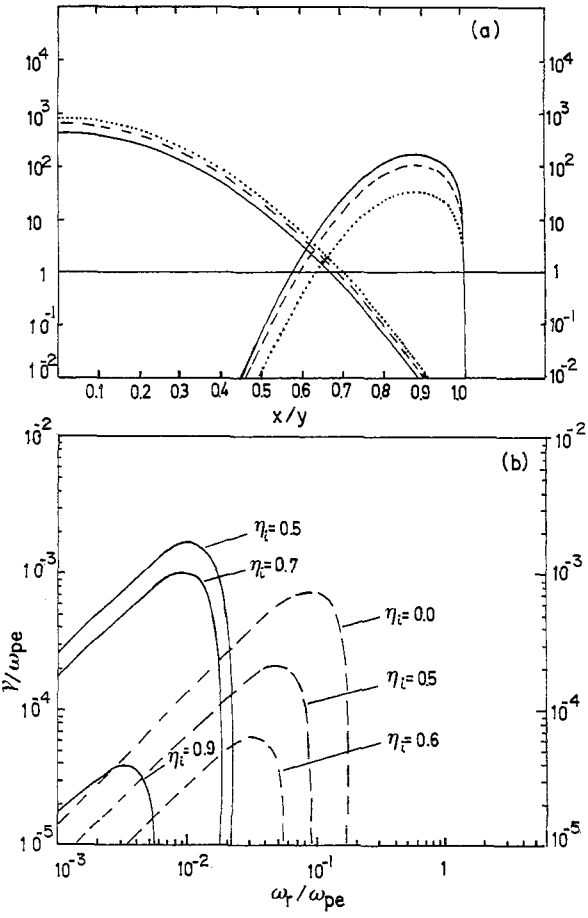

FIG. 9.—(a) The same as Fig. 8(a) but for $\eta_i = 0.5$ (——), 0.7 (— —) and 0.9 (. . . . .). (b) Growth rates versus frequency normalized to ω_{pe}. For $\theta = 75°$ (——), $\eta_i = 0.5, 0.7, 0.9$ and for $\theta = 0°$ (— —), $\eta_i = 0.6, 0.5, 0.0$. The other parameters are the same as in Fig. 1.

We have taken $\theta = 75°$, for which the dominant instability is the ion–ion acoustic instability.

We have increased and reduced the drift velocity by a factor of 10. When the drift velocity is reduced, the beam term opens up, as shown in Fig. 10(a), in such a way that for $U/\alpha_b = 2.5$ it becomes larger than the other terms everywhere. This means that the waves are damped. In other words, decreasing drift velocities stabilize the two unstable modes. On the other hand, increasing beam velocities make the ion beam and the ion core terms shrink, as shown in the figure. As a result of the shrinkage, the instability, which for $U/\alpha_b = 25$ is the ion–ion acoustic instability, is now dominated by the other mode, i.e. the ion acoustic instability. This effect is shown in Fig. 10(b), where we clearly see the decrease of the growth rate due to increasing drift velocities until it starts increasing again, but now as the ion acoustic mode, whose largest growth rate occurs for $\theta = 0°$.

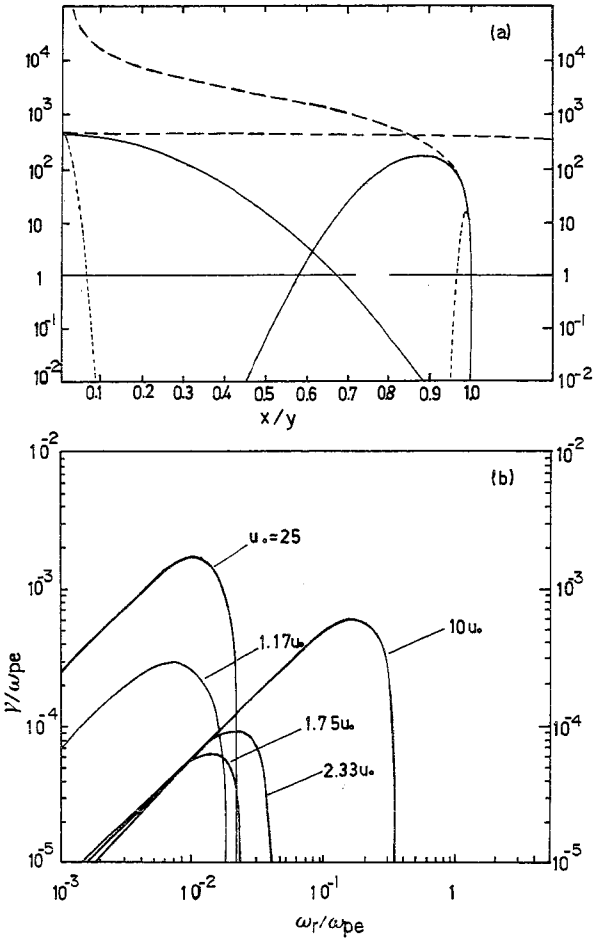

FIG. 10.—(a) The same as Fig. 1 for $\theta = 75°$. The drift velocity has been increased (– – – –) and reduced (— —) by a factor of 10. (b) Growth rate for increasing drift velocity from $u_0 = (U/\alpha_b) = 25$ to $10u_0$.

According to previous considerations, one would expect that increasing the angle beyond 75° could trigger again the ion–ion acoustic mode. This is in fact so, because the effect of increasing the angle reflects itself in that the ion core and beam terms open up in such a way that for sufficiently large angles, they can intersect each other above the electronic term.

To this end, in Fig. 11(a) we take the same plasma model as in Fig. 10(a) for the largest beam velocity case, i.e. $(U/\alpha_b) = 250$ and $\theta = 90°$. We see that the two ionic terms intersect each other at a value 60 times larger than the electron term. Thus, we expect the ion–ion mode to dominate. Figure 11(b) shows the growth rates for the same plasma model as in Fig. 11(a) for $\theta = 60°$, 75° and 89°. We clearly see that even for 75°, the dominant mode is the ion acoustic instability, but for 89° the other mode, i.e. the ion–ion acoustic instability, is dominant.

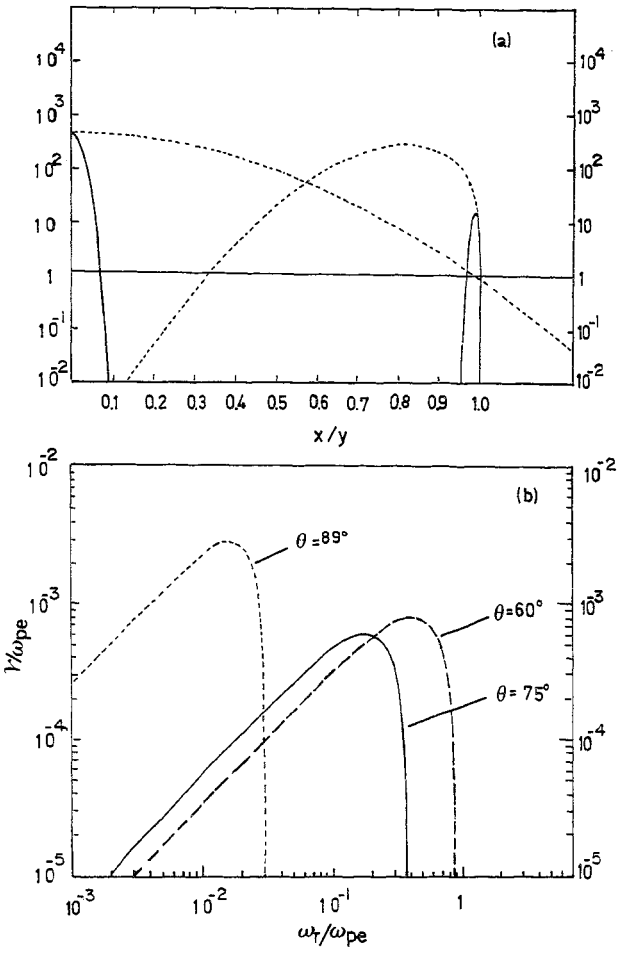

FIG. 11.—(a) The same as Fig. 1(a) for $(U/\varkappa_b) = 250$, and $\theta = 75°$ (——) and 89° (– – – –). (b) Growth rates for the plasma model of Fig. 11(a) for $\theta = 60°$ (— —), 75° (——) and 85° (– – – –).

To summarize, we can say that the two modes are destabilized by increasing the relative drift velocity, but the angular threshold of the ion–ion instability is shifted to larger angles.

4. THE ION ACOUSTIC MODE

Although we have derived analytical expressions for the dispersion relation and the growth rate, equations (3) and (4), they are a set of coupled equations which, as they stand, must be solved numerically. However, when the mode is the ion acoustic instability, it is possible to simplify the equations by noticing that such an instability occurs for $x \simeq y$.

Thus, setting in equation (3) $x \simeq y$ and noting that the last two terms of this

equation are of importance only around the maximum growth rate of the ion–ion acoustic instability, we obtain the following equation for $(x-y)$:

$$y = -2\left(\frac{U}{\alpha_e}\cos\theta\right)^2 + \frac{\delta\eta_b}{\left(1-\frac{x}{y}\right)^2}\left[1+\frac{3}{2}\frac{1}{\left(1-\frac{x}{y}\right)^2\left(\frac{U}{\alpha_b}\cos\theta\right)^2}\right] + \delta\eta_i\left[1+\frac{3}{2}\frac{1}{\left(\frac{U}{\alpha_i}\cos\theta\right)^2}\right]. \quad (10)$$

From equation (4), we obtain

$$\frac{\gamma}{\omega_{pe}} = \frac{\sqrt{\pi}\, x\left(\frac{U}{\alpha_e}\cos\theta\right)^3}{\left\{\frac{\eta_b\delta}{\left(1-\frac{x}{y}\right)^3}\left(1+\frac{3}{\left(1-\frac{x}{y}\right)^2\left(\frac{U}{\alpha_b}\cos\theta\right)^2}\right)-\delta\eta_i\right\}}. \quad (11)$$

The two equations have thus been decoupled, and can now be solved. From equation (10) we obtain

$$(y-x)^2 = \frac{1}{2}\frac{\delta\eta_b y^2}{y^2+2\left(\frac{U}{\alpha_e}\cos\theta\right)^2-\delta\eta_i} - \left\{1+\left[1+\frac{6}{\delta\eta_b\left(\frac{U}{\alpha_b}\cos\theta\right)^2}\left(y^2+2\frac{U}{\alpha_p}\cos^2\theta-\delta\eta_b\right)\right]^{1/2}\right\}. \quad (12)$$

Since the ion acoustic instability is maximum for parallel propagation and for small angles, $U/\alpha_b \gg 1$, equation (10) can be approximated by

$$\omega_r = k_\parallel U - \frac{C_s}{\sqrt{2}}\left(\frac{n_b}{n_e}\right)^{1/2} k_\parallel\left\{1+\left(1+12\frac{n_e}{n_b}\frac{T_b}{T_e}\right)^{1/2}\right\}, \quad (13)$$

where $C_s = (T_e/M_i)^{1/2}$ is the ion sound speed.

Under the same conditions, equation (11) reduces to

$$\frac{\gamma}{\omega_{pe}} = \frac{\sqrt{\pi}\, x (U/\alpha_e)^3 \cos^3\theta}{\left(\dfrac{\delta\eta_b}{\left(1-\dfrac{x}{y}\right)^3} - \delta\eta_i \right)}. \tag{14}$$

For $\theta = 0^\circ$ and $T_b \ll T_e$, equations (13) and (14) yield

$$\omega_r = kU - \left(\frac{n_b}{n_e}\right)^{1/2} c_s k, \tag{15}$$

and

$$\gamma = \sqrt{\pi}\, \frac{c_s}{\alpha_e} \left(\frac{n_b}{n_e}\right)^{1/2} kU, \tag{16}$$

which are the same equations derived by GRABBE and EASTMAN (1984), DUSENBERY and LYONS (1985) and ASHOUR-ABDALLA and OKUDA (1986).

It is interesting to notice that in a purely cold plasma, the dominant mode is always the instability due to the relative drift between the electrons and the ion beam. The mode due to the relative drift between the ion core and the ion beam is completely negligible which follows from the cold plasma dispersion relation:

$$1 = \frac{1}{x^2} + \frac{\delta\eta_i}{x^2} + \frac{\delta\eta_b}{(x-y)^2}. \tag{17}$$

In fact, the second term on the right-hand side of this equation represents the ion core and, as we see, is negligible compared to the first term which represents the electrons.

The maximum growth rate can be calculated from equation (17) and is given by (see e.g. CUPERMAN *et al.*, 1978):

$$\gamma_{max} = \frac{\sqrt{3}}{2} \left(\frac{\delta\eta_b}{2}\right)^{1/3}. \tag{18}$$

Thus, although decreasing ion core and ion beam temperatures have a destabilizing effect on both modes, decreasing the electron plasma temperature stabilizes the ion–ion mode.

5. SUMMARY

We have shown that the exact dispersion relation, equation (1), can be approximated by equations (3) and (4) for $\omega/k\alpha_i > 1$, and by equations (6) and (7) for $\omega/k\alpha_i < 1$. This has been done by assuming that $\omega_r \gg \gamma$. This assumption is justified *a posteriori* by noticing that maximum growth rates are always at least one order of magnitude less than the corresponding frequency. The other assumptions involved in

the derivation of the analytical expressions for the dispersion relation and growth rate, depend on the external parameters used. Sometimes, however, $\omega/k\alpha_i$ becomes of the order one close to the marginal frequency, but since our analytical expressions reduce to equation (5) at the marginal frequency and this equation is an exact relation, we conclude that even then the approximations yield the right results. We then compared the growth rates calculated from the exact dispersion relation, equation (1), with the growth rates given by our analytical results and the agreement was very good. Nevertheless, since equations (3) and (4) constitute a system of algebraic coupled equations which besides describe two electrostatic modes, it is not easy to separate the main effects leading to each mode. However, when the analytical results are complemented with the condition for marginal instability, equation (5), the effects leading to each instability can be clearly discerned.

In particular, it follows from our analysis that the maximum growth rate of the ion–ion acoustic instability is about one order of magnitude larger than that of the ion acoustic instability, as a result of the large value reached by the ion background Landau term. In fact, from the figures and the corresponding analysis, it follows that whenever the growth rate of the ion–ion acoustic instability reaches its largest value, the difference between the ion background and the ion beam Landau terms is at least one order of magnitude larger than the electron term. Moreover, since the growth rate of the instability is proportional to the sum of the Landau kinetic terms, it follows that the instability grows to large values due to the ion background Landau term and therefore, it is a resonant kinetic-like instability which is in agreement with the conclusion reached by DUSENBERY and LYONS (1985) (see also DUSENBERY, 1988 and references therein).

For the plasma parameters used in the figures, the ion–ion acoustic instability dominates over the ion acoustic instability at large angles. However, it can dominate at any angle. This is most easily seen by noticing that the dispersion relation depends on the drift velocity U, and the propagation angle θ, only through the product $U\cos\theta$. Therefore, if for a given drift velocity $U = U_0$, the largest growth rate occurs for an angle $\theta = \theta_0$, then by reducing the beam velocity to $U = U_0\cos\theta_0$, the same maximum occurs for $\theta = 0°$. By the same argument it follows that changes in the beam velocity can only change the angle at which the growth rate of the ion–ion acoustic instability reaches the largest value, but the actual value remains unaltered. For the ion acoustic instability, the same argument shows that increasing beam velocities lead to an enhancement of the maximum growth rates. In fact, the same growth rate for $\theta = 0°$ occurs for larger angles when the drift velocity is increased and, since the fastest growing waves propagate in a direction parallel to the beam direction, we conclude that maximum growth rates are enhanced by increasing drift velocities. These results also follow from Figs 10 and 11.

Decreasing values of the beam temperature enhance the unstable frequency range and the growth rate of both instabilities, and also increases the angular threshold of the ion–ion acoustic mode, i.e. it becomes dominant at larger angles.

A decrease of the ion background temperature has a destabilizing effect on the ion–ion acoustic instability and a negligible effect on the ion acoustic mode.

The ion–ion acoustic instability is maximum for $\eta_i = \eta_b = 0.5$, while the ion acoustic instability is maximum for $\eta_i = 0$.

Most of the aforementioned results can be found in the literature. They have been

obtained using numerical methods. However, the method employed here is new and provides a simple way of understanding the nature of the two unstable modes and their dependence on the various parameters involved.

Acknowledgements—This paper was supported in part by the Comisión Nacional de Investigación Científica y Tecnológica, grant 0001/88; and by the Departamento Técnico de Investigación de la Universidad de Chile, grant E 2812/8812.

REFERENCES

AKIMOTO K. and OMIDI N. (1986) *Geophys. Res. Lett.* **13**, 97.
ASHOUR-ABDALLA M. and OKUDA H. (1986) *J. Geophys. Res.* **91**, 6833.
CUPERMAN S., GOMBEROFF L. and ROTH I. (1978) *J. Plasma Phys.* **19**, 1.
DUSENBERY P. B. (1986) *J. Geophys. Res.* **91**, 12.005.
DUSENBERY P. B. (1987) *J. Geophys. Res.* **92**, 2560.
DUSENBERY P. B. (1988) *J. Geophys. Res.* **93**, 14.729.
DUSENBERY P. B. and LYONS (1985) *J. Geophys. Res.* **90**, 10935.
FORSLUND D. W. and SHONK C. R. (1970) *Phys. Rev. Lett.* **25**, 281.
FRIED B. D. and CONTE S. (1961) *The Plasma Dispersion Function*. Academic Press, NY.
FRIED B. D. and WONG A. Y. (1966) *Physics Fluids* **9**, 1084.
GARY P. S. and OMIDI N. (1987) *J. Plasma Phys.* **37**, 41.
GRABBE C. L. (1987) *J. Geophys. Res.* **92**, 1185.
GRABBE C. L. and EASTMAN T. E. (1984) *J. Geophys. Res.* **89**, 3865.
GRESILLON D., DOVEIL F. and BUZZI J. M. (1975) *Phys. Rev. Lett.* **34**, 197.
GURNETT D. A. and FRANK L. A. (1977) *J. Geophys. Res.* **82**, 1031.
GURNETT D. A. and FRANK L. A. (1978) *J. Geophys. Res.* **83**, 58
OMIDI N. (1985) *J. Geophys. Res.* **90**, 12330.
OMIDI N. and AKIMOTO K. (1988) *J. Geophys. Res.* **93**, 14.725.
SCARF F., FRANK L., ACKERSON K. and LEPPING R. (1974) *Geophys. Res. Lett.* **1**, 189.
STRINGER T. E. (1964) *Plasma Phys.* **6**, 267.